THE ROLES OF BOUNDARY-LAYER DYNAMICS ON THE DEVELOPMENT OF MADDEN-JULIAN OSCILLATION*

Chao Jiping (巢纪平),

National Research Center for Marine Environment Forecasts, Beijing 100081

Lin Yonghui (林永辉)

Institute of Atmospheric Physics, Chinese Academy of Sciences, Beijing 100029

and *Wang Bin* (王 斌)

Department of Meteorology, University of Hawaii, Hawaii, USA

Received August 18, 1994; revised October 20, 1994

ABSTRACT

In this paper, a tropical atmospheric model of relevance to short-term climate variations (Wang and Li 1993) is utilized for study of the development of Madden-Julian oscillation. The model contains an interactive process of boundary-layer Ekman convergence and precipitation heating. The model is solved by expanding dependent variables in terms of parabolic cylindrical functions in the meridional direction and truncating three meridional modes $n=0, 2, 4$ for equatorial symmetric solutions. The free wave solutions obtained under long-wave approximation are induced as a Kelvin wave and two Rossby waves. After considering the effect of boundary-layer dynamic process, the modified Kelvin wave becomes unstable in long-wave bands with a typical growth rate on an order of 10^{-6} s^{-1} and an eastward phase speed of 10 m s^{-1}; the most unstable mode is wavenumber one. These theoretical results are consistent with the observed Madden-Julian oscillation in equatorial area. For the two modified Rossby waves, one with a smaller meridional scale ($n=4$) decays except for extra long-waves; the other with a larger meridional scale ($n=2$) grows in short-wave bands. This may be relevant to explaining the westward propagation of super cloud clusters in the Madden-Julian oscillation. The theory suggests that the boundary-layer dynamic process is an important mechanism in the development of the Madden-Julian oscillation.

Key words: Madden-Julian oscillation, intraseasonal oscillation, boundary-layer convergence

I. INTRODUCTION

The 40—50 day (sometimes termed 30—60 day or intraseasonal) oscillation discovered by Madden and Julian (1971; 1972) is one of the fundamental components of the tropical atmospheric circulation. On the one hand, this oscillation reflects internal dynamics of the tropical atmosphere; on the other hand, it is likely one of either the phases of ENSO or the trigger mechanisms of ENSO development. Therefore, a large number of studies on Madden-Julian oscillation (MJO, hereafter) were paid attention in the last decade. Based on the analysis of observed data, many essential features of the MJO are revealed. First, the MJO exhibits a global zonal scale (more than 10 000 km) in tropics, and contains a multi-scale structure composed of

* This work is supported by the National Natural Science Foundation of China.

a few super cloud clusters which have a horizontal scale of 1000 km. Second, the principal circulation of the MJO moves eastward along the equator and amplifies over the warm waters of equatorial Indian and western Pacific Oceans, whereas the individual cloud clusters can move unstably westward along the equator. Last, the vertical structure of the MJO is dominated by the gravest baroclinic mode; the horizontal structure appears to be characterized by a coupled Kelvin–Rossby wave.

In theoretical studies, many researchers have followed the train of thought of wave–CISK (conditional instability of the second kind) mechanism and emphasized the interaction between the equatorial Kelvin wave–induced moisture convergence and the convective heating (Chang 1977; Lau and Peng 1987; Chang and Lim 1988). Although the Kelvin wave–CISK mechanism can be responsible for the slowly eastward propagation of MJO, it does not explain the global–scale instability; the most unstable waves are short–waves. If the latent heating is nonlinear, small–scale disturbances remain most unstable (Wang and Xue 1992), although the nonlinear heating favors a narrow precipitation region and a global–scale circulation. In this sense, no matter it is linear or nonlinear, the wave–CISK mechanism can not explain the planetary–scale of the MJO.

Emanuel (1987) proposed an evaporation–wind feedback mechanism for explaining the MJO. Even in the absence of equatorial Kelvin wave, the east–west asymmetry in evaporational heating can induce a slowly eastward–moving Walker–type circulation cell in a uniform easterly basic flow. However, similar to wave–CISK mechanism, the instability still favors the high–wavenumber disturbances.

Wang (1988) considered that the Ekman pumping–induced moisture convergence and the wave–induced moisture convergence are not the same in phase, so the heating due to the boundary–layer moisture convergence gives rise to an instability favorable for planetary scales (Wang and Chen 1989). This mechanism will be referred to as Ekman convergence–precipitation heating feedback. After considering the Ekman convergence–precipitation heating feedback, Wang (1993) made a numerical experiment by solving initial–value problem. Initially, an equatorially trapped easterly Kelvin wave perturbation is centered around the equator with a zonal scale of 4000 km and a cosine structure. The time integration indicates that as initial Kelvin wave perturbation continuously moves eastward, a new Kelvin wave perturbation is excited in front of (or down–stream) the major cell; at the same time, Rossby wave perturbations with a scale of 1000 km form behind (or up–stream) the major cell and present an equator–symmetric structure; therefore the full circulation is presented as a coupled Kelvin–Rossby wave structure. The results are very consistent with the observation of the MJO.

In this paper, we will discuss the eigenvalues and eigenvectors of the model of short–term climate variations (Wang and Li 1993) in order to better understand the development of the MJO in terms of the dispersion and instability of the disturbance.

II. THE MODEL

The present model (Wang and Li 1993) consists of a well–mixed planetary boundary layer and a free troposphere represented by the gravest baroclinic mode. The precipitation heating is described by the CISK–type cumulus parameterization. The supply of lower–layer moisture is provided by the convergence of boundary–layer flows. If the non–uniformity of sea (or land) surface temperature distribution is not considered, the governing equations for the

free–troposphere written on an equatorial β–plane with long–wave approximation are

$$\frac{1}{C_0^2}\frac{\partial \varphi}{\partial t} + (1-I)\left(\frac{\partial u}{\partial x} + \frac{\partial v}{\partial y}\right) + d(1-B)\left(\frac{\partial u_B}{\partial x} + \frac{\partial v_B}{\partial y}\right) = 0, \tag{1}$$

$$\beta y u = -\frac{\partial \varphi}{\partial y}, \tag{2}$$

$$\frac{\partial u}{\partial t} - \beta y v = -\frac{\partial \varphi}{\partial x}, \tag{3}$$

where $C_0^2 \equiv \frac{1}{2} S_0 (P_s / P_2)^2 \triangle P^2$ is the gravity wave speed for the gravest baroclinic mode; $I \equiv \frac{RbL_c}{C_p P_2 S_2 \triangle p}(\bar{q}_3 - \bar{q}_1)$ is the heating coefficient due to free–troposphere moisture convergence; $S_2 \equiv S_0 (P_s / P_2)^2$ is the static stability parameter in the middle of the free troposphere; $B \equiv (RbL_c \bar{q}_e) / (C_p P_2 S_2 \triangle p)$ is the heating coefficient due to boundary–layer moisture convergence, $d \equiv (P_s - P_e) / \triangle p$ is the depth of the boundary–layer; $f \equiv \beta y$ is the equatorial β–plane approximation; φ is the geopotential height in the lower free troposphere; (u, v) and (u_B, v_B) are the horizontal velocity in the lower free troposphere and boundary–layer, respectively.

The governing equations for boundary–layer are

$$\beta y u_B = -\frac{\beta y}{E_0^2 + \beta^2 y^2}\left(\beta y \frac{\partial \varphi}{\partial y} + E_0 \frac{\partial \varphi}{\partial x}\right), \tag{4}$$

$$\delta \frac{\partial u_B}{\partial t} - \beta y v_B = -\frac{\beta y}{E_0^2 + \beta^2 y^2}\left(\beta y \frac{\partial \varphi}{\partial x} - E_0 \frac{\partial \varphi}{\partial y}\right), \tag{5}$$

where $E_0 \equiv \rho_s g K_D / (P_s - P_e)$ is the Ekman number of the boundary–layer, δ is the switch–on parameter:

$$\delta = \begin{cases} 1, & \text{non} - \text{steady boundary} - \text{layer} \\ 0. & \text{steady boundary} - \text{layer} \end{cases}$$

The detailed description can be found in Wang and Li (1993).

For convenience, we introduce the following characteristic and nondimensional variables:

$$\begin{cases} (x,y) = \left(\frac{C_0}{2\beta}\right)^{\frac{1}{2}}(x^*, y^*), \\ t = T_0 t^* = (2\beta C_0)^{-\frac{1}{2}} t^*, \\ \varphi = C_0^2 \varphi^*, \\ (u,v;\ u_B, v_B) = C_0 (u^*, v^*;\ u_B^*, v_B^*). \end{cases} \tag{6}$$

The nondimensional governing equations for the motions in the present coupled free troposphere–boundary–layer model are derived from Eqs. (1)—(5) (the superscript " * " is omitted hereafter):

$$\frac{\partial \varphi}{\partial t} + (1-I)\left(\frac{\partial u}{\partial x} + \frac{\partial v}{\partial y}\right) + d(1-B)\left(\frac{\partial u_B}{\partial x} + \frac{\partial v_B}{\partial y}\right) = 0, \tag{7}$$

$$\frac{1}{2}yu = -\frac{\partial\varphi}{\partial y}, \tag{8}$$

$$\frac{\partial u}{\partial t} - \frac{1}{2}yv = \frac{\partial\varphi}{\partial x}, \tag{9}$$

$$\frac{1}{2}yu_B = -\frac{y}{4E^2+y^2}\left(y\frac{\partial\varphi}{\partial y} + 2E\frac{\partial\varphi}{\partial x}\right), \tag{10}$$

$$\delta\frac{\partial u_B}{\partial t} - \frac{1}{2}yv_B = -\frac{y}{4E^2+y^2}\left(y\frac{\partial\varphi}{\partial x} - 2E\frac{\partial\varphi}{\partial y}\right), \tag{11}$$

where $E = E_0 T_0$.

From Eqs. (8) and (9) the divergence of free-troposphere satisfies:

$$\frac{\partial u}{\partial x} + \frac{\partial v}{\partial y} = -\frac{4}{y^2}\left(\frac{1}{2}\frac{\partial\varphi}{\partial x} + \frac{\partial^3\varphi}{\partial t\partial y^2} - \frac{2}{y}\frac{\partial^2\varphi}{\partial t\partial y}\right). \tag{12}$$

Similar to Eq. (12), from Eqs. (10) and (11) the divergence of boundary-layer satisfies:

$$\frac{\partial u_B}{\partial x} + \frac{\partial v_B}{\partial y} =$$

$$-\frac{4}{(4E^2+y^2)^2}\left\{\delta\left[(4E^2+y^2)\left(\frac{\partial^2}{\partial y^2} + \frac{2E}{y}\frac{\partial^2}{\partial x\partial y} - \frac{2E}{y^2}\frac{\partial}{\partial x}\right) - 2y\left(\frac{\partial}{\partial y} + \frac{2E}{y}\frac{\partial}{\partial x}\right)\right]\frac{\partial\varphi}{\partial t}\right.$$

$$\left. -\frac{1}{2}(4E^2-y^2)\frac{\partial\varphi}{\partial x} - 2Ey\frac{\partial\varphi}{\partial y} + E(4E^2+y^2)\left(\frac{\partial^2\varphi}{\partial x^2} + \frac{\partial^2\varphi}{\partial y^2}\right)\right\}. \tag{13}$$

Substituting (12) and (13) into Eq. (7), the thermodynamic equation of the free troposphere is

$$\left\{(4E^2+y^2)[(4E^2+y^2)(1-I) + \delta d(1-B)y^2]\frac{\partial^2}{\partial y^2}\right.$$

$$-2[(4E^2+y^2)^2(1-I) + \delta d(1-B)y^4]\frac{1}{y}\frac{\partial}{\partial y} + 2\delta d(1-B)E(4E^2+y^2)y\frac{\partial^2}{\partial x\partial y}$$

$$\left. -2\delta dE(1-B)(4E^2+3y^2)\frac{\partial}{\partial x} - \frac{1}{4}(4E^2+y^2)^2y^2\right\}\frac{\partial\varphi}{\partial t} + \frac{1}{2}\left[(4E^2+y^2)^2(1-I)\right.$$

$$\left. -d(1-B)(4E^2-y^2)y^2\right]\frac{\partial\varphi}{\partial x} - 2d(1-B)Ey^3\frac{\partial\varphi}{\partial y}$$

$$+d(1-B)Ey^2(4E^2+y^2)\left(\frac{\partial^2\varphi}{\partial x^2} + \frac{\partial^2\varphi}{\partial y^2}\right) = 0. \tag{14}$$

Eq. (14) is the governing equation (or model) for our study. The high-frequency inertial gravity waves are filtered out by the long-wave approximation.

If $d=0$ and $E=0$, Eq. (14) is simplified as

$$\left[(1-I)\left(\frac{\partial^2}{\partial y^2} - \frac{2}{y}\frac{\partial}{\partial y}\right) - \frac{1}{4}y^2\right]\frac{\partial\varphi}{\partial t} + \frac{1}{2}(1-I)\frac{\partial\varphi}{\partial x} = 0. \tag{15}$$

In the absence of heating ($I=0$), Eq. (15) is Matsuno (1966) equation with the long-wave approximation. Eq. (15) describes the eastward propagating Kelvin wave and the westward propagating Rossby waves. We will refer to these moist waves as free waves.

III. WEBER FUNCTIONS EXPANSION AND TRUNCATED EQUATIONS

Eq. (14) is solved by expanding dependent variables in terms of the parabolic cylindrical functions (i.e. Weber functions). φ is expanded into the following form:

$$\varphi = \sum_{n=0}^{\infty} \varphi_n(x,t) D_n(y), \tag{16}$$

where $D_n(y)$ is the parabolic cylinderical function of order n. Using the properties of Weber functions and considering the integration:

$$\int_{-\infty}^{\infty} \mathrm{e}^{-ay^2}\,\mathrm{d}y = \sqrt{\frac{\pi}{a}}. \tag{17}$$

One can readily obtain the integration in the form of $\int_{-\infty}^{\infty} y^{2m} \mathrm{e}^{-ay^2}\,\mathrm{d}y$ $(m=1, 2, \cdots)$, and prove that:

$$\int_{-\infty}^{\infty} D_m(y) D_n(y)\,\mathrm{d}y = \begin{cases} n!\ \sqrt{2\pi}, & (n=m) \\ 0. & (n \neq m) \end{cases} \tag{18}$$

Substituting (16) into Eq. (14), taking the truncated modes $n=0$, 2, 4 for equatorial even–symmetric solutions, Eq. (14) leads to

$$\begin{aligned} &\left(a_{00}\frac{\partial \varphi_0}{\partial t} + b_{00}\frac{\partial^2 \varphi_0}{\partial t \partial x} + c_{00}\frac{\partial \varphi_0}{\partial x} + d_{00}\frac{\partial^2 \varphi_0}{\partial x^2} + e_{00}\varphi_0\right) \\ &+\left(a_{02}\frac{\partial \varphi_2}{\partial t} + b_{02}\frac{\partial^2 \varphi_2}{\partial t \partial x} + c_{02}\frac{\partial \varphi_2}{\partial x} + d_{02}\frac{\partial^2 \varphi_2}{\partial x^2} + e_{02}\varphi_2\right) \\ &+\left(a_{04}\frac{\partial \varphi_4}{\partial t} + b_{04}\frac{\partial^2 \varphi_4}{\partial t \partial x} + c_{04}\frac{\partial \varphi_4}{\partial x} + d_{04}\frac{\partial^2 \varphi_4}{\partial x^2} + e_{04}\varphi_4\right) = 0, \end{aligned} \tag{19}$$

$$\begin{aligned} &\left(a_{20}\frac{\partial \varphi_0}{\partial t} + b_{20}\frac{\partial^2 \varphi_0}{\partial t \partial x} + c_{20}\frac{\partial \varphi_0}{\partial x} + d_{20}\frac{\partial^2 \varphi_0}{\partial x^2} + e_{20}\varphi_0\right) \\ &+\left(a_{22}\frac{\partial \varphi_2}{\partial t} + b_{22}\frac{\partial^2 \varphi_2}{\partial t \partial x} + c_{22}\frac{\partial \varphi_2}{\partial x} + d_{22}\frac{\partial^2 \varphi_2}{\partial x^2} + e_{22}\varphi_2\right) \\ &+\left(a_{24}\frac{\partial \varphi_4}{\partial t} + b_{24}\frac{\partial^2 \varphi_4}{\partial t \partial x} + c_{24}\frac{\partial \varphi_4}{\partial x} + d_{24}\frac{\partial^2 \varphi_4}{\partial x^2} + e_{24}\varphi_4\right) = 0, \end{aligned} \tag{20}$$

$$\begin{aligned} &\left(a_{40}\frac{\partial \varphi_0}{\partial t} + b_{40}\frac{\partial^2 \varphi_0}{\partial t \partial x} + c_{40}\frac{\partial \varphi_0}{\partial x} + d_{40}\frac{\partial^2 \varphi_0}{\partial x^2} + e_{40}\varphi_0\right) \\ &+\left(a_{42}\frac{\partial \varphi_2}{\partial t} + b_{42}\frac{\partial^2 \varphi_2}{\partial t \partial x} + c_{42}\frac{\partial \varphi_2}{\partial x} + d_{42}\frac{\partial^2 \varphi_2}{\partial x^2} + e_{42}\varphi_2\right) \\ &+\left(a_{44}\frac{\partial \varphi_4}{\partial t} + b_{44}\frac{\partial^2 \varphi_4}{\partial t \partial x} + c_{44}\frac{\partial \varphi_4}{\partial x} + d_{44}\frac{\partial^2 \varphi_4}{\partial x^2} + e_{44}\varphi_4\right) = 0, \end{aligned} \tag{21}$$

where the coefficients a_{ij}, b_{ij}, c_{ij}, d_{ij}, e_{ij} $(i,j=0, 2, 4)$ are given in Appendix 1.

IV. EIGENVALUES AND EIGENVECTORS

The solutions of Eqs. (19)—(21) are given by

$$(\varphi_0,\varphi_2,\varphi_4)=(\Phi_0,\Phi_2,\Phi_4)e^{i(kx-\sigma t)}. \tag{22}$$

Substituting (22) into (19)—(21) then yields

$$\overline{A}X=\sigma\overline{B}X, \tag{23}$$

where $X=(\Phi_0,\Phi_2,\Phi_4)^T$, (24)

$$\overline{A}=\begin{bmatrix} C_{00}k+ik^2d_{00}-ie_{00} & C_{02}k+ik^2d_{02}-ie_{02} & C_{04}k+ik^2d_{04}-ie_{04} \\ C_{20}k+ik^2d_{20}-ie_{20} & C_{22}k+ik^2d_{22}-ie_{22} & C_{24}k+ik^2d_{24}-ie_{24} \\ C_{40}k+ik^2d_{40}-ie_{40} & C_{42}k+ik^2d_{42}-ie_{42} & C_{44}k+ik^2d_{44}-ie_{44} \end{bmatrix}, \tag{25}$$

$$\overline{B}=\begin{bmatrix} a_{00}+ikb_{00} & a_{02}+ikb_{02} & a_{04}+ikb_{04} \\ a_{20}+ikb_{20} & a_{22}+ikb_{22} & a_{24}+ikb_{24} \\ a_{40}+ikb_{40} & a_{42}+ikb_{42} & a_{44}+ikb_{44} \end{bmatrix}. \tag{26}$$

Therefore, the eigenvalues σ of Eqs. (19)—(21) can be obtained by solving the matrix:

$$\overline{A}=\sigma\overline{B}. \tag{27}$$

After finding out the three eigenvalues and corresponding eigenvectors (Φ_0,Φ_2,Φ_4), combining Eqs. (22), (16) with (8), (9), (10), (11), one can compute the distributions of φ, u, v and u_B, v_B.

The standard parameter values used in the model are given in Table 1.

Table 1. Standard Parameter Values

Parameter	Standard values	Parameter	Standard values
I	0.18	B	2.4
d	0.375	E	0.015
C_0	30 (m s^{-1})		

V. THE DYNAMIC EFFECTS OF A STEADY BOUNDARY-LAYER

1. *Free Waves*

Figure 1 is the dispersion relation of the free waves without considering the dynamic effect of the steady boundary-layer. It contains three waves; one is eastward-moving Kelvin wave denoted by K; the other two are westward-moving Rossby waves, in which one with a larger meridional scale is signified as R_1 and the other with a smaller meridional scale is signified as R_2.

2. *The Phase Speed and Growth Rate*

As the parameters take the standard values shown in Table 1, with the presence of the dynamic process of a steady boundary-layer, the waves (shown in Fig. 2) are named as the

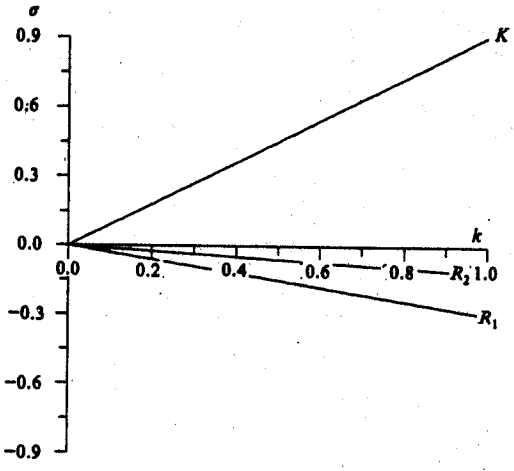

Fig. 1. The dispersion relation of the model free waves under long–wave approximation ($I=0.18$).

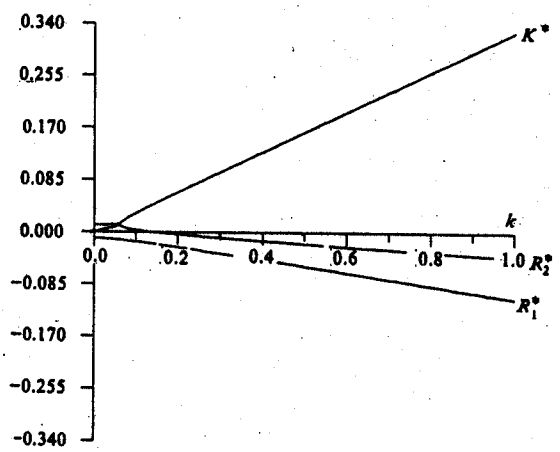

Fig. 2. The phase speed of the steady boundary–layer moisture convergence–precipitation heating feedback mode.

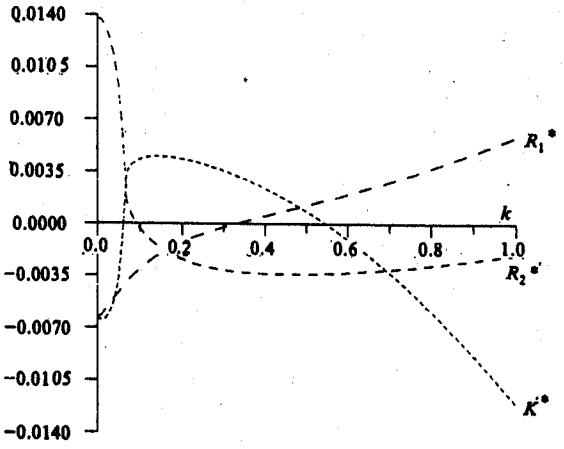

Fig. 3. The growth rate of the steady boundary–layer moisture convergence–precipitation heating feedback mode.

modified Kelvin and Rossby waves denoted by K^*, R_1^*, R_2^* respectively. Figure 2 indicates that the phase speeds of the modified waves are becoming smaller; furthermore, the modified Rossby wave with a small meridional scale (R_2^*) converts into eastward–propagation in extra long–waves.

Figure 3 indicates that the eastward modified Kelvin wave (K^*) becomes unstable for long–waves due to the effect of boundary–layer Ekman convergence–precipitation heating. The most unstable wave appears in $k=0.14$ (i.e. corresponding to zonal wavenumber one). Combined with Fig. 2, the corresponding eastward phase speed is about 10 m s^{-1} and the period is about 45 days. The e–fold time for the amplification is about 69 days. For the two modified

Rossby waves, one with a smaller meridional scale (R_2^*) decays except for extra long-waves; but the other with a larger meridional sacle (R_1^*) grows in short-wave bands. It is deduced that the wave (R_1^*) reflects the unstable westward movement of tropical cloud clusters.

3. *The Dependence of Phase Speed and Growth Rate on the Parameters*

No matter how the parameters B and E vary, the modified Kelvin wave for $k=0.14$ always propagates eastward (Fig. 4a), and its phase speed increases with increasing B and E. The modified Rossby wave R_1^* always propagates westward, and the phase speed also increases with increasing B and E. More interesting, the modified Rossby wave R_2^* may propagate from westward to eastward in reverse order with increasing B, the greatest eastward propagating speed occurs when the parameters B and E take some intermediate values.

As shown in Fig. 5a, the growth of the eastward modified Kelvin wave can appear in a broad parameter domain, within which, the modified Rossby wave R_2^* decays. The mode

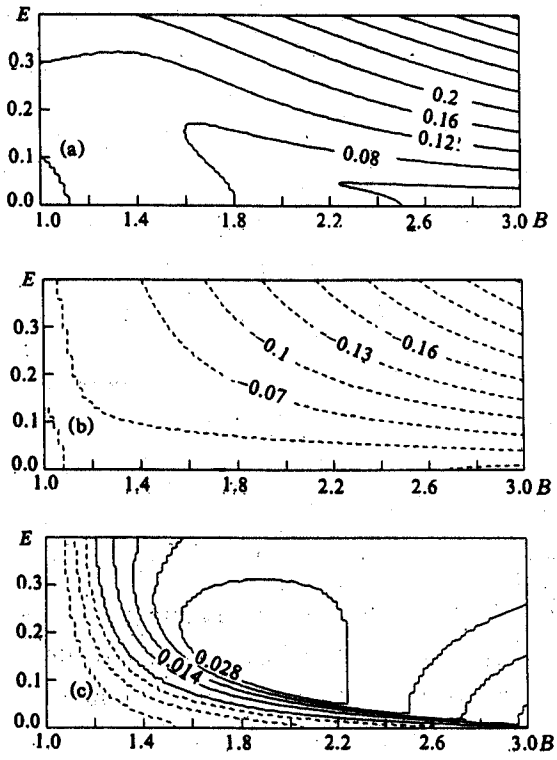

Fig. 4. The phase speed as functions of B and E for (a) modified Kelvin wave (K^*), (b) modified Rossby wave with a larger meridional scale (R_1^*) and (c) modified Rossby wave with a smaller meridional scale (R_2^*). In the computation, $k=0.14$ and a steady boundary-layer is assumed.

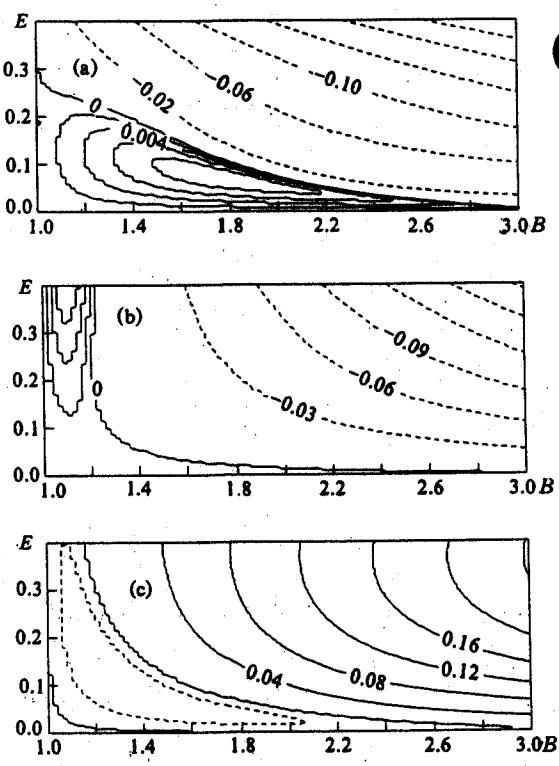

Fig. 5. As in Fig. 4 but for growth rate.

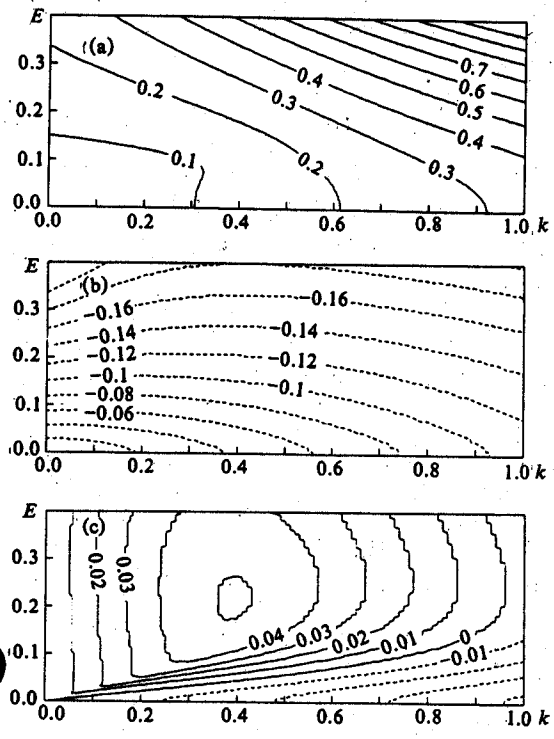

Fig. 6. The phase speed as functions of k and E for (a) modified Kelvin wave (K^*), (b) modified Rossby wave (R_1^*) and (c) modified Rossby wave (R_2^*). In the computation, $B=2.4$ and a steady boundary–layer is assumed.

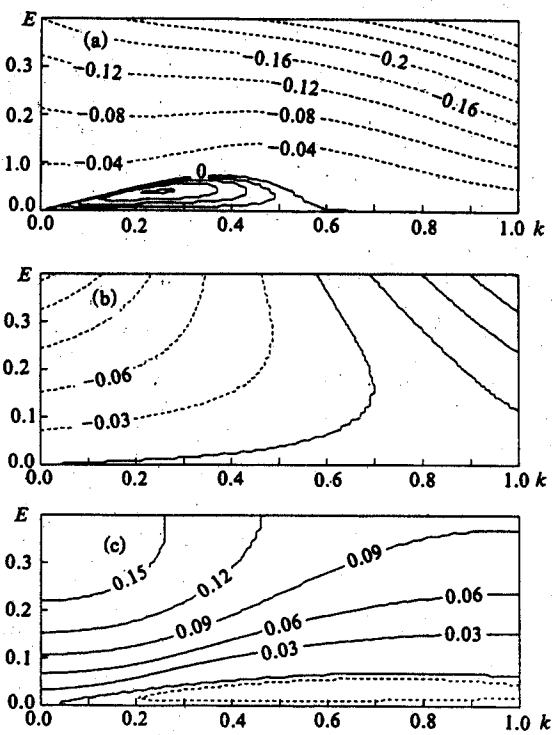

Fig. 7. As in Fig. 6 but for growth rate.

R_2^* may be unstable if B and E exceed certain critical values. The modified Rossby wave R_1^* may be unstable when B is small. These results indicate that the model contains both the unstable eastward–progagating and unstable westward–propagating modes.

When B is fixed and takes the value of 2.4, the dependence of the dispersion relation of the three modified waves on E and k is shown in Fig. 6. The modified Kelvin wave is always eastward–propagating; its phase speed increases with increasing E. The modified Rossby wave R_1^* always propagates westward and the phase speed also increases with increasing E. The modified Rossby wave R_2^* propagates westward when E is small, but it propagates eastward when E exceeds the certain values. Figure 6c also indicates that the stationary wave moves toward short–waves with increasing E.

Similar to Fig. 6, when B is fixed and takes the value of 2.4, the dependence of growth and decay rates of the three modified waves on E and k is shown in Fig. 7. Only if the parameter E takes small values and $k<0.6$, the modified Kelvin wave is unstable. The most unstable wave emerges as k takes the value of 0.2 to 0.3. For the modified Rossby wave R_1^*, long–waves decay and short–waves grow. The growth rate increases with increasing E. This indicates that the role

of frictional process is not always negative when both damping process and the boundary–layer convergence are considered in a unified model. For another modified Rossby wave R_2^*, the wave is unstable when E takes reasonable values, especially for long–waves. It is seen from Fig. 6c and Fig. 7c that as E takes appropriate values, the modified Rossby wave R_2^* may grow and move eastward. However since its phase speed is an order of magnitude smaller than that of the modified Kelvin wave, the principal circulation is dominated by the modified Kelvin wave.

As the parameter E is fixed and takes the value of 0.015, the dependence of the dispersion relation of the three modified waves on B and k is shown in Fig. 8. The modified Kelvin wave always propagates eastward. The modified Rossby wave R_1^* always propagates westward. The modified Rossby wave R_2^*, however, is eastward–propagating in extra long–wave bands as B takes large values. This is consistent with Fig. 2. Corresponding growth and decay rates are shown in Fig. 9. For the modified Kelvin waves, long–waves are unstable, but when B is large enough and the wavelength is very long, the modified Kelvin wave may decay. The most unstable wave occurs as $k=0.14$ and $B=2.4$. The modified Rossby wave R_1^* is unstable in part of short–waves, but it decays in part of long–waves and the critical wavelength of decay decreases with increasing B. The modified Rossby wave R_2^* is unstable when B is small; as B takes large values, only the extra long–waves are unstable.

4. *The Structure and Evolution of Physical Fields*

The structures of the modified Kelvin wave, modified Rossby waves and the coupled

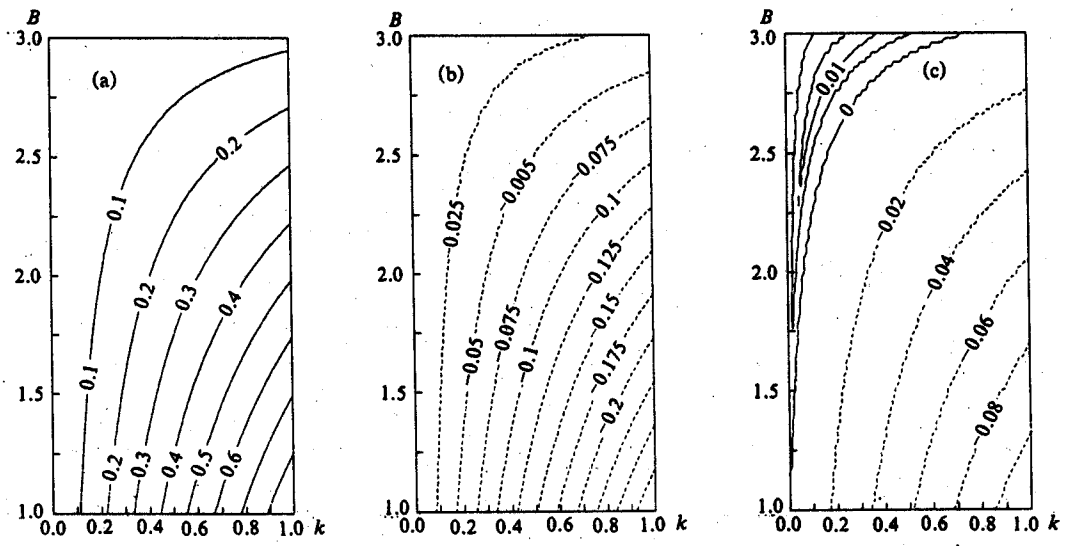

Fig. 8. The phase speed as functions of k and B for (a) modified Kelvin wave (K^*), (b) modified Rossby wave (R_1^*) and (c) modified Rossby wave (R_2^*). In the computation, $E=0.015$ and a steady boundary–layer is assumed.

Kelvin–Rossby wave are shown in Figs. 10a—10d, respectively.

The longitude–time diagram of the geopotential field summed up by the three eigenvectors (as k takes the value of 0.14) is shown in Fig. 11. The low–frequency wave slowly moves eastward along the equator. Its phase speed is consistent with the observed Madden–Julian oscillation, about 10 m s^{-1}, and its amplitude increases with time.

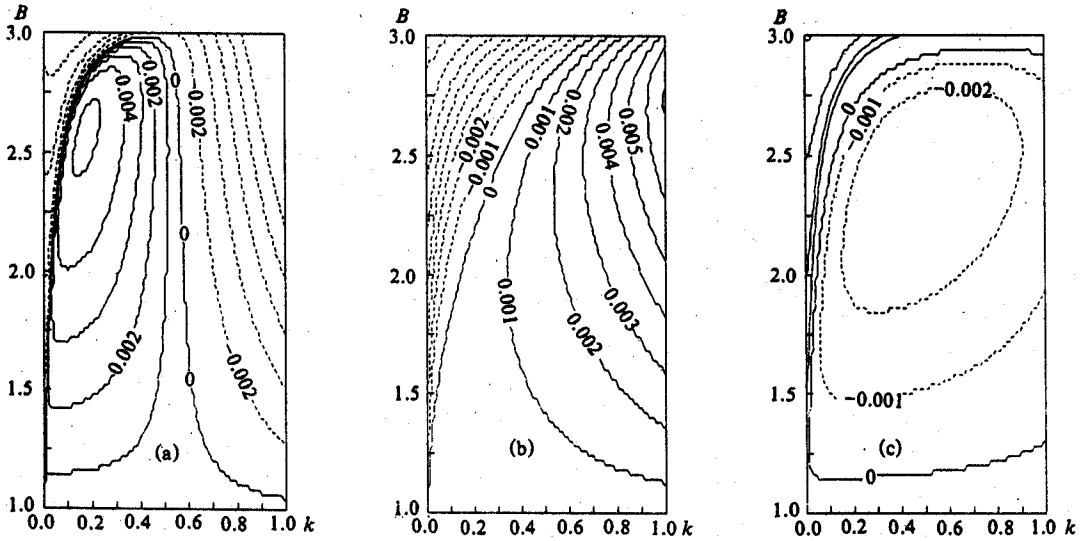

Fig. 9. As in Fig. 8 but for growth rate.

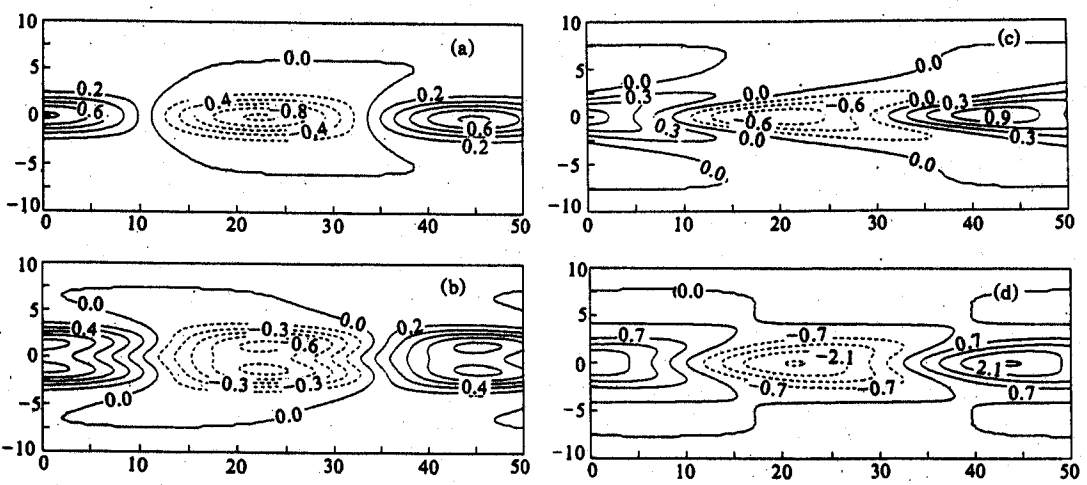

Fig. 10. The geopotential height of the eigenvector corresponding to (a) modified Kelvin wave (K^*), (b) modified Rossby wave (R_1^*), (c) modified Rossby wave (R_2^*) and (d) composite structure of above three modes. The ordinate is latitude in degree and the abscissa is zonal dimensionless length.

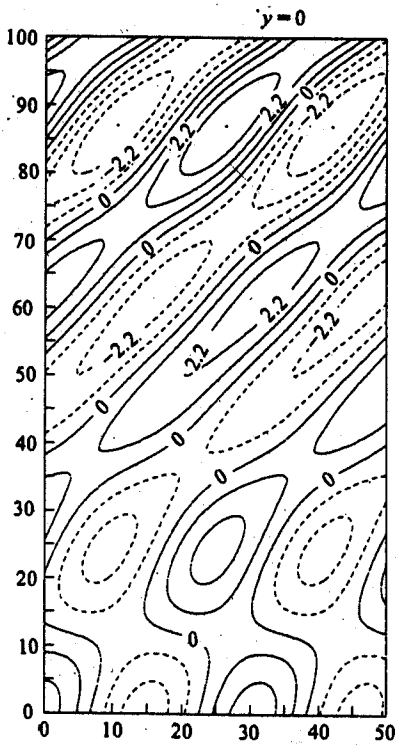

Fig. 11. Longitude–time diagram of the geopotential in the lower free troposphere along the equator. The abscissa is zonal dimensionless length and the ordinate is time in day.

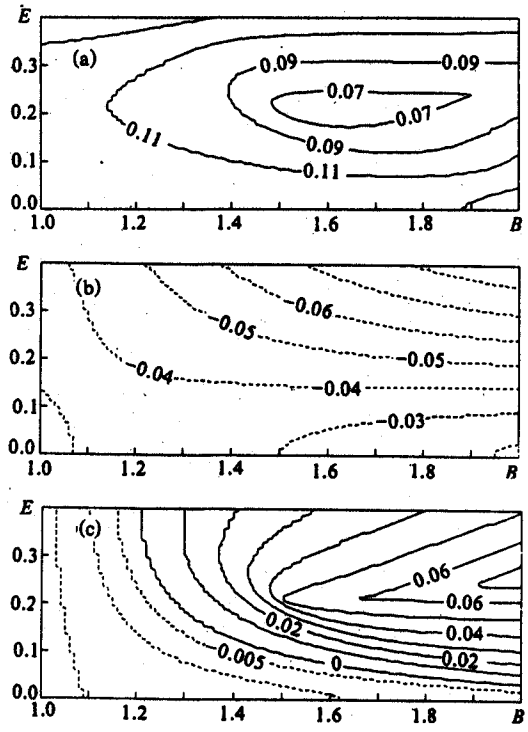

Fig. 12. As in Fig.4 but that the results are obtained for a non–steady boundary–layer.

VI. THE DYNAMIC EFFECT OF A NON–STEADY BOUNDARY–LAYER

Here, we briefly discuss the dynamic effect of a non–steady boundary–layer (i. e. $\delta=1$) moisture convergence on Madden–Julian oscillation. Comparing with Fig. 4, the modified Kelvin wave of $k=0.14$ still moves eastward, but the slowest wave emerges when $E=0.2$ and $B=1.7$ due to the dynamic effect of non–steady boundary–layer (Fig. 12a). The modified Rossby wave R_1^* still moves westward, but its phase speed is about 50% slower than that shown in Fig. 4a. Another modified Rossby wave R_2^* is eastward–propagating when B and E take large values and its phase speed is about 50% greater than that shown in Fig. 4c; as B and E take small values the wave moves westward.

The corresponing growth (decay) rate is shown in Fig. 13. As $k=0.14$, the dependence of growth rate of the modified Kelvin wave on B and E has a remarkable change. The growth rate has a discontinuity and is very sensitive to the parameters near the discontinuity. At the same time, the most unstable region occurs when B takes large values and the unstable growth rate is an order of magnitude larger than that in a steady boundary–layer. The modified Rossby wave R_2^* also has the feature of discontinuity. When B takes large values there exist both large growth and decay rate. For the same B, the wave is growing when E takes large values, and is

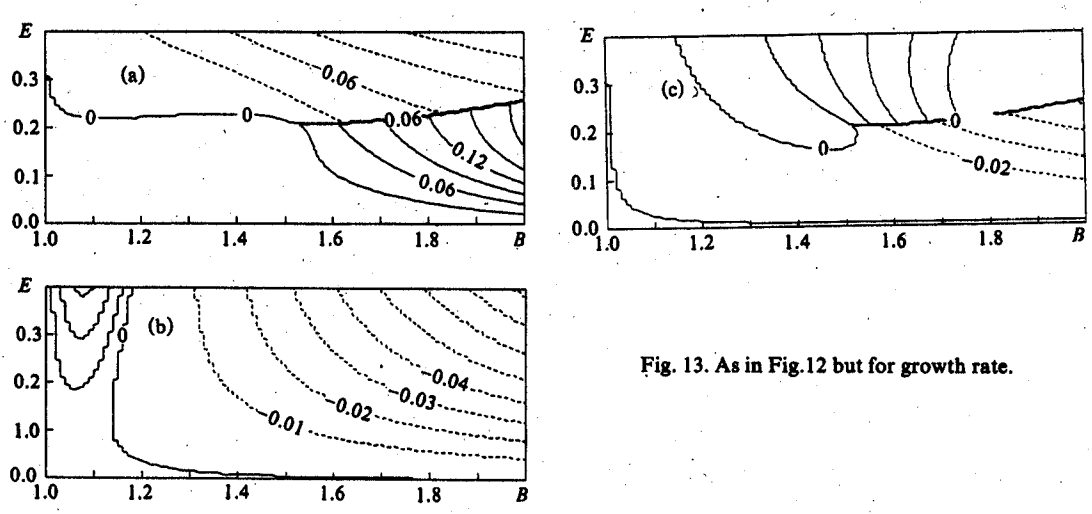

Fig. 13. As in Fig.12 but for growth rate.

decaying when E takes small values. This is qualitatively consistent with the characteristics of the R_2^* mode in a steady boundary–layer. For the modified Rossby wave R_1^*, its dependence on the parameters is the same as that in a steady boundary–layer.

VII. CONCLUSIONS

Based on the preceding analyses, the following conclusions are obtained:

(1) After considering the dynamic effect of boundary–layer, the modified Kelvin wave becomes unstable in long–wave bands, its typical growth rate with an order of 10^{-6} s^{-1} and an eastward phase speed of about 10 m s^{-1}, the most unstable mode is wavenumber–one.

(2) The modified Rossby wave with larger meridional scale is unstable in the short–wave bands as reasonable parameter values are taken; this is maybe relevant to explaining the westward–propagation of super cloud clusters. The modified Rossby wave with a smaller meridional scale may move eastward and become unstable in extra long–wave bands.

(3) The physical field represented by the combination of three modified waves exhibits a strucrure of a coupled Kelvin–Rossby wave. The field (or principal circulation) moves eastward along the equator.

In summary, after considering the large–scale dynamic effect of the boundary–layer, the theoretical results can qualitatively reflect principal observed features of Madden–Julian oscillation. In this model, we did not consider the wave–CISK (i. e. $I< 1$) and the evaporation–wind feedback process. Therefore, this paper suggests a new unstable mechanism on the development of Madden–Julian oscillation. It deserves further investigations. Certainly, the truncation ($N=0$, 2, 4) may affect the results, but comparing with the results of Wang (1993), the conclutions are qualitatively believable.

APPENDIX 1

$$a_{00} = \frac{15}{4}[\delta d(1-B) - I] + \delta d(1-B)\left(\frac{3}{2} + E^2\right) - E^2 I(6 + 4E^2) + (1-I)\left(\frac{3}{2} + 4E^2 + 8E^4\right)$$

$$b_{00} = -3\delta dE(1-B)(3+4E^2)$$

$$c_{00} = (1-I)\left(\frac{3}{2}+4E^2+8E^4\right)+d(1-B)\left(\frac{3}{2}-2E^2\right)$$

$$d_{00} = d(1-B)E(3+4E^2)$$

$$e_{00} = d(1-B)E\left(\frac{21}{4}+E^2\right)$$

$$a_{02} = \frac{45}{2}[\delta d(1-B)-I]-\delta d(1-B)(30+8E^2)-8E^2I(3+E^2)-(1-I)(30+56E^2-64E^4)$$

$$b_{02} = -4\delta dE(1-B)(3-2E^2)$$

$$c_{02} = (1-I)(6+8E^2)+d(1-B)(6-4E^2)$$

$$d_{02} = 4(1-B)dE(3+2E^2)$$

$$e_{02} = -d(1-B)E\left(\frac{15}{2}+8E^2\right)$$

$$a_{20} = \frac{45}{2}[\delta d(1-B)-I]+\delta d(1-B)(6+8E^2)-8E^2I(3+E^2)+(1-I)(6+8E^2)$$

$$b_{20} = -8\delta d(1-B)E(3+E^2)$$

$$c_{20} = (1-I)(6+8E^2)+d(1-B)(6-4E^2)$$

$$d_{20} = 4Ed(1-B)(3+2E^2)$$

$$e_{20} = d(1-B)E\left(\frac{57}{2}+8E^2\right)$$

$$a_{22} = \frac{375}{2}[\delta d(1-B)-I]-\delta d(1-B)(165+22E^2)-E^2I(156+40E^2)-(1-I)(165+184E^2+48E^4)$$

$$b_{22} = -\delta d(1-B)E(90+24E^2)$$

$$c_{22} = (1-I)(39+40E^2+16E^4)+d(1-B)(39-20E^2)$$

$$d_{22} = d(1-B)E(78+40E^2)$$

$$e_{22} = d(1-B)E\left(\frac{45}{2}-22E^2\right)$$

$$a_{04} = 90[\delta d(1-B)-I]-\delta d(1-B)(132-24E^2)-48E^2I-(1-I)(132-256E^4)$$

$$b_{04} = 24\delta dE(1-B)$$

$$c_{04} = 12(1-I)+12d(1-B)$$

$$d_{04} = 24d(1-B)E$$

$$e_{04} = -d(1-B)E(42-24E^2)$$

$$a_{24} = 1170[\delta d(1-B)-I]-\delta d(1-B)(1608+96E^2)-E^2I(672+96E^2)-(1-I)(1608+1056E^2+256E^4)$$

$$b_{24} = -\delta dE(1-B)(48-96E^2)$$

$$c_{24} = (1-I)(168+96E^2)+d(1-B)(168-48E^2)$$

$$d_{24} = d(1-B)E(336+96E^2)$$

$$e_{24} = -d(1-B)E(438+96E^2)$$

$$a_{40} = 90[\delta d(1-B)-I]+\delta d(1-B)(12+24E^2)-48E^2I+12(1-I)$$

$$b_{40} = -24\delta d(1-B)E$$

$$c_{40} = 12(1-I)+12d(1-B)$$

$$d_{40} = 24dE(1-B)$$

$$e_{40} = d(1-B)E(102+24E^2)$$

$$a_{42} = 1170[\delta d(1-B)-I]-\delta d(1-B)(600-96E^2)-E^2I(672+96E^2)-(1-I)(600+288E^2)$$

$$b_{42} = -\delta d(1-B)E(384+96E^2)$$

$$c_{42} = (1-I)(168+96E^2)+d(1-B)(168-48E^2)$$

$$d_{42} = d(1-B)E(336+96E^2)$$

$$e_{42} = d(1-B)E(570+96E^2)$$

$$a_{44} = 11610[\delta d(1-B)-I]-\delta d(1-B)(12132+936E^2)-E^2I(5904+864E^2)-(1-I)(12132+7584E^2-312E^4)$$

$$b_{44} = -\delta dE(1-B)(1944+288E^2)$$

$$c_{44} = (1-I)(1476+864E^2+192E^4)+d(1-B)(1476-432E^2)$$

$$d_{44} = d(1-B)E(2952+864E^2)$$

$$e_{44} = -d(1-B)E(1026+936E^2)$$

REFERENCES

Chang, C. P. (1977), Viscous internal gravity waves and low frequency oscillation in the tropics, *J. Atmos. Sci.*, **34:** 901—910.

Chang, C. P. and Lim, H. (1988), Kelvin wave–CISK: A possible mechanism for the 30—50 day oscillation, *J. Atmos. Sci.*, **45:** 1709—1720.

Emanuel, K. A. (1987), An air–sea interaction model of intraseasonal oscillation in the tropics, *J. Atmos. Sci.*, **44:** 2324—2340.

Lau, K. –M. and Peng, L. (1987), Origin of low frequency (intraseasonal) oscillation in the tropical atmosphere, Part I: The basic theory, *J. Atmos. Sci.*, **44:** 950—972.

Madden, R. A. and Julian, P. R. (1971), Detection of a 40—50 day oscillation in the zonal wind in the tropical Pacific, *J. Atmos. Sci.*, **28:** 702—708.

Madden, R. A. and Julian, P. R. (1972), Description of global–scale circulation cells in the tropics with a 40—50 day period, *J. Atmos. Sci.*, **29:** 1109—1123.

Matsuno, T. (1966), Quasi–geostraphic motions in the equatorial area, *J. Meteor. Soc. Japan*, **44:** 25—43.

Wang, B. (1988), Dynamics of tropical low–frequency waves: An analysis of the moist Kelvin wave, *J. Atmos. Sci.*, **45:** 2051—2065.

Wang, B. (1993), Dynamics of Madden–Julian Oscillation, *Trends in the Atmospheric Sciences*, **1:** 349—373.

Wang, B. and Chen, J. K. (1989), On the zonal scale selection and vertical structure of the equatorial intraseasonal waves, *Quart. J. Roy. Meteor. Soc.*, **115:** 1301—1323.

Wang, B. and Li, T. (1993), A simple tropical atmosphere model of relevance to short–term climate variations, *J. Atmos. Sci.*, **50:** 260—284.

Wang, B. and Xue, Y. (1992), On the behavior of a moist Kelvin wave packet with nonlinear heating, *J. Atmos. Sci.*, **49:** 549—559.